**PATTER, Volume *1***

## Supplemental Information

# Intelligent Electromagnetic Sensing with Learnable Data Acquisition and Processing

**Hao-Yang Li, Han-Ting Zhao, Meng-Lin Wei, Heng-Xin Ruan, Ya Shuang, Tie Jun Cui, Philipp del Hougne, and Lianlin Li**

## Supplementary Note 1. Sensing system based on the programmable metasurface

The configuration of proposed intelligent sensing system, with reference to **Figure 1a** in main text, consists of a pair of horn antennas, a vector network analyzer (VNA, Aligent E5071C), and a large-aperture programmable metasurface. The operational principle of the presented sensing system is described as following. Antenna 1, connected to port-1 of VNA, is used to emit periodically microwave illumination signals, which are shaped by the m-ANN-driven programmable metasurface. After being scattered by the subject of interest, the wavefield shaped by the metasurface are received by Antenna-2 connected to port-2 of VNA. Finally, the received microwave raw data are instantly processed by the r-ANN, producing the desired imaging or recognition results.

**Figures S1a** show the photos of the front and back views of the designed programmable metasurface. For the sake of fabrication limitation, the whole metasurface is designed to be composed of $3\times 4$ identical metasurface panels, and each panel has $8 \times 8$ meta-atoms. Each meta-atom has a size of $54\times54\text{mm}^2$, thus the whole metasurface has a size of $1.7\times1.3\text{m}^2$ in total. The metasurface is electronically controlled with a FPGA-based Micro-Control-Unit (MCU), as shown in the insert of **Figure S1a**. In addition, the geometrical parameters of the electronically-controllable digital meta-atom are detailed in **Figure S1b.** From **Figure S1c,** each metasurface panel is equipped with eight 8-bit shift registers (SN74LV595APW), and every 8 PIN diodes share a shift register. With the use of shift registers, 8 PIN diodes are sequentially controlled. The MCU sends the commands over 24 independent branch channels, leading to real-time manipulations of all PIN diodes. The MCU works with one common clock (CLK) signal. In our work, the adopted CLK is 50MHz, and the switching time of PIN diode is about 10us each cycle. We remark that the control strategy can be extended for more PIN diodes by concatenating more metasurface

panels in a straightforward manner, allowing adjustable rearrangement of metasurface panels for various application needs.

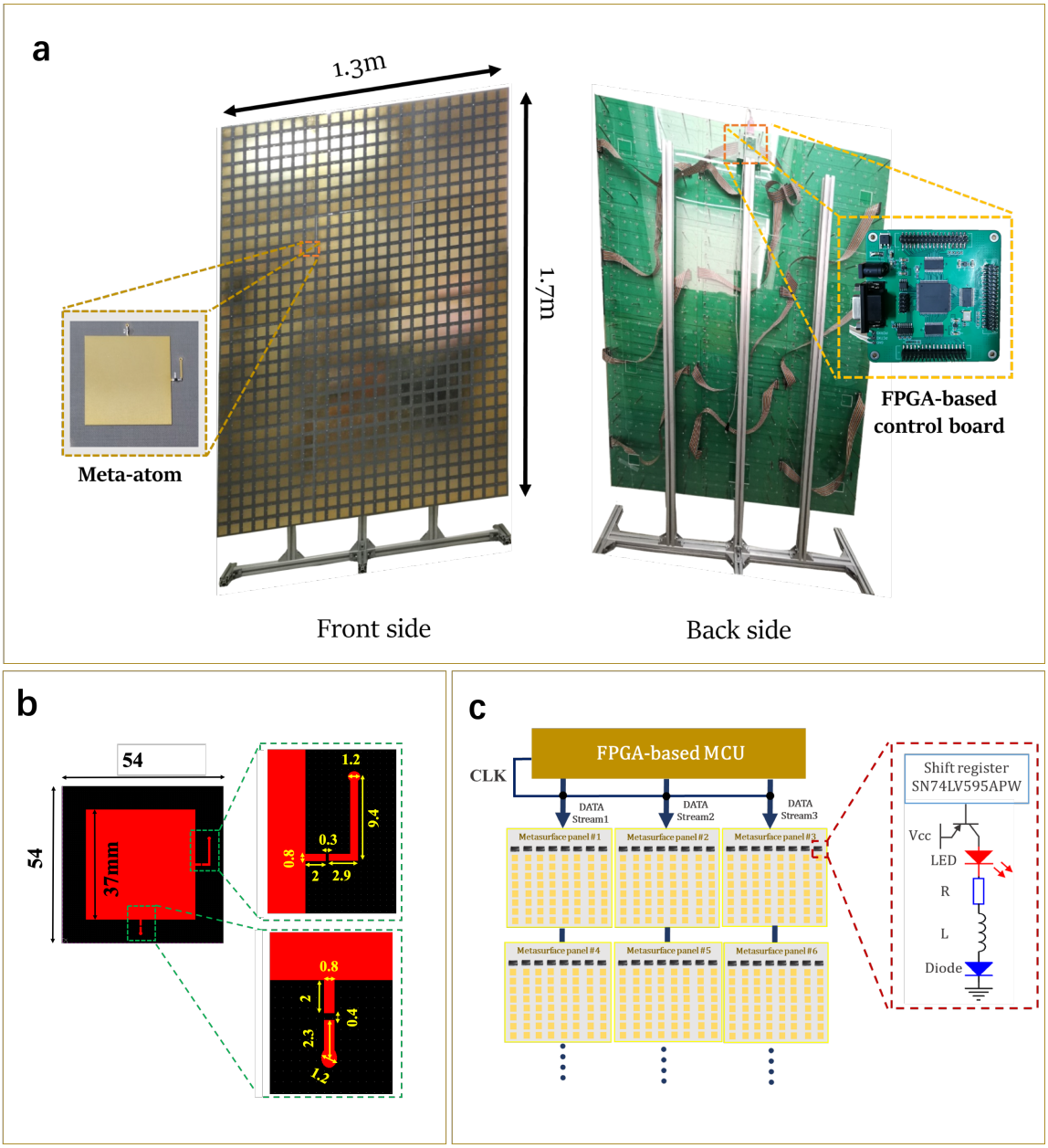


**Figure S1**. **(a),** the photos of front-side and back-side of the designed programmable metasurface. Here, the FPGA-based micro control unit (MCU) has been inserted as well in the back-side view picture. **(b)** the geometrical parameters of the designed electronically-controllable meta-atom of the metasurface. **(c)** the illustrative control strategy of the programmable metasureface.

## Supplementary Note 2. Discussions about the VAE objective function

In this note, we would like to discuss briefly Eq. (1) outlined in main text, and elaborate on associated optimization algorithm. Generally speaking, the measurement procedure of the proposed intelligent sensing strategy can be viewed as an end-to-end process that given a scene $\boldsymbol{x}$ (image or class label of probed subject) generates a set of measurements $\boldsymbol{y}$ by sampling from a $\boldsymbol{\mathcal{C}}$-controllable conditional distribution $\boldsymbol{y}\sim q_{\boldsymbol{\mathcal{C}}}(\boldsymbol{y}|\boldsymbol{x},\boldsymbol{\Theta})$, where $\boldsymbol{\mathcal{C}}$ encapsulates all trainable parameters of the hardware setting, i.e., the user-controlled coding pattern of metasurface in our work. This conditional distribution is known as the likelihood in the framework of Bayesian analysis, and can be understood as a stochastic measurement model. Basically, the goal of data processing pipeline is to produce an estimate $\hat{\boldsymbol{x}}$ of the scene $\boldsymbol{x}$ given the measurements $\boldsymbol{y}$. Basically, the estimator $\hat{\boldsymbol{x}}$ serves as an inverse action of the measurement process, and can be realized with a deep ANN with network weights $\boldsymbol{\Phi}$. Similar to the measurement process, we denote the estimator with a parametric conditional distribution $\hat{\boldsymbol{x}}\sim p(\hat{\boldsymbol{x}}|\boldsymbol{y},\boldsymbol{\Phi})$. We propose to simultaneously learn the learnable parameters, i.e., $\boldsymbol{\mathcal{C}}$ and $\boldsymbol{\Phi}$, of both the measurement process and the reconstruction operator in context of VAE, such as to optimize the whole sensing performance in a specific task. In light of VAE, the optimal choices of $\boldsymbol{\mathcal{C}}$ and $\boldsymbol{\Phi}$ can be achieved by minimizing the following objective function, i.e.,

$$\mathcal{L}(\boldsymbol{\mathcal{C}},\boldsymbol{\Phi}) = -\mathbb{E}_{q_{\boldsymbol{\mathcal{C}}}(\boldsymbol{y}|\boldsymbol{x},\boldsymbol{\Theta})}[\log p(\boldsymbol{x}|\boldsymbol{y},\boldsymbol{\Phi})] + \mathrm{KL}(q_{\boldsymbol{\mathcal{C}}}(\boldsymbol{y}|\boldsymbol{x},\boldsymbol{\Theta})||p(\boldsymbol{y})) \tag{S1}$$

Note that the mathematic expectation in the first term of the right hand of Eq. (S1) is taken over the distribution $q_{\boldsymbol{\mathcal{C}}}(\boldsymbol{y}|\boldsymbol{x},\boldsymbol{\Theta})$, which embodies the $\boldsymbol{\mathcal{C}}$-controllable measurements and the reconstruction network as a whole. In a nutshell, this term serves as a likelihood, which is used to measure the reconstruction error over $q_{\boldsymbol{\mathcal{C}}}(\boldsymbol{y}|\boldsymbol{x},\boldsymbol{\Theta})$. In contrast, the second term is characterized by KL-divergence, which, as a regu larizer, encourages the measurement distribution $q_{\boldsymbol{\mathcal{C}}}(\boldsymbol{y}|\boldsymbol{x},\boldsymbol{\Theta})$ to be close to a chosen prior $p(\boldsymbol{y})$. Here, $p(\boldsymbol{y})$ is chosen to be

zero-mean Gaussian distribution with maximum Shannon information entropy. As such, each measurement is optimized to capture as much information of the probed scene as possible.

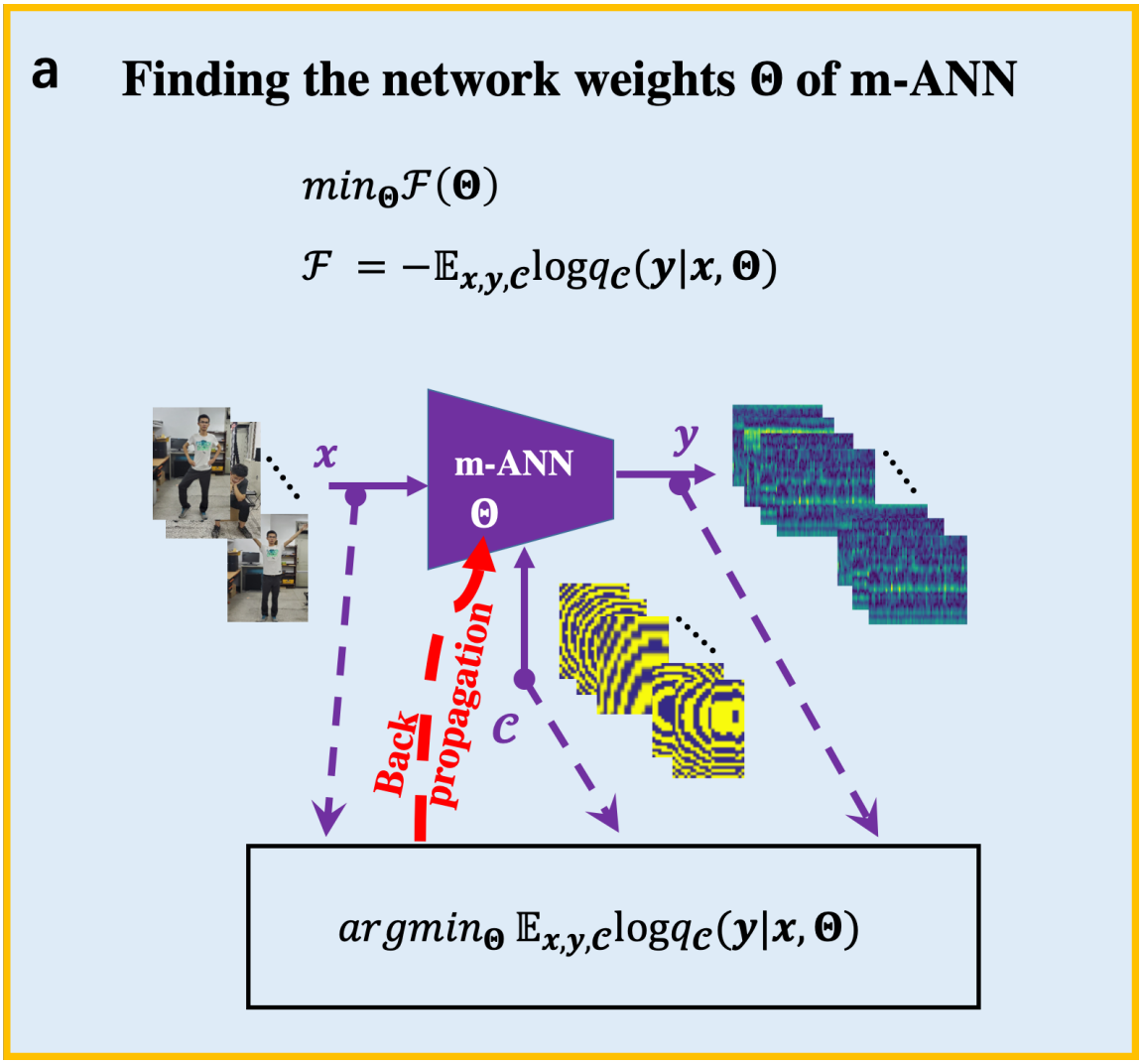

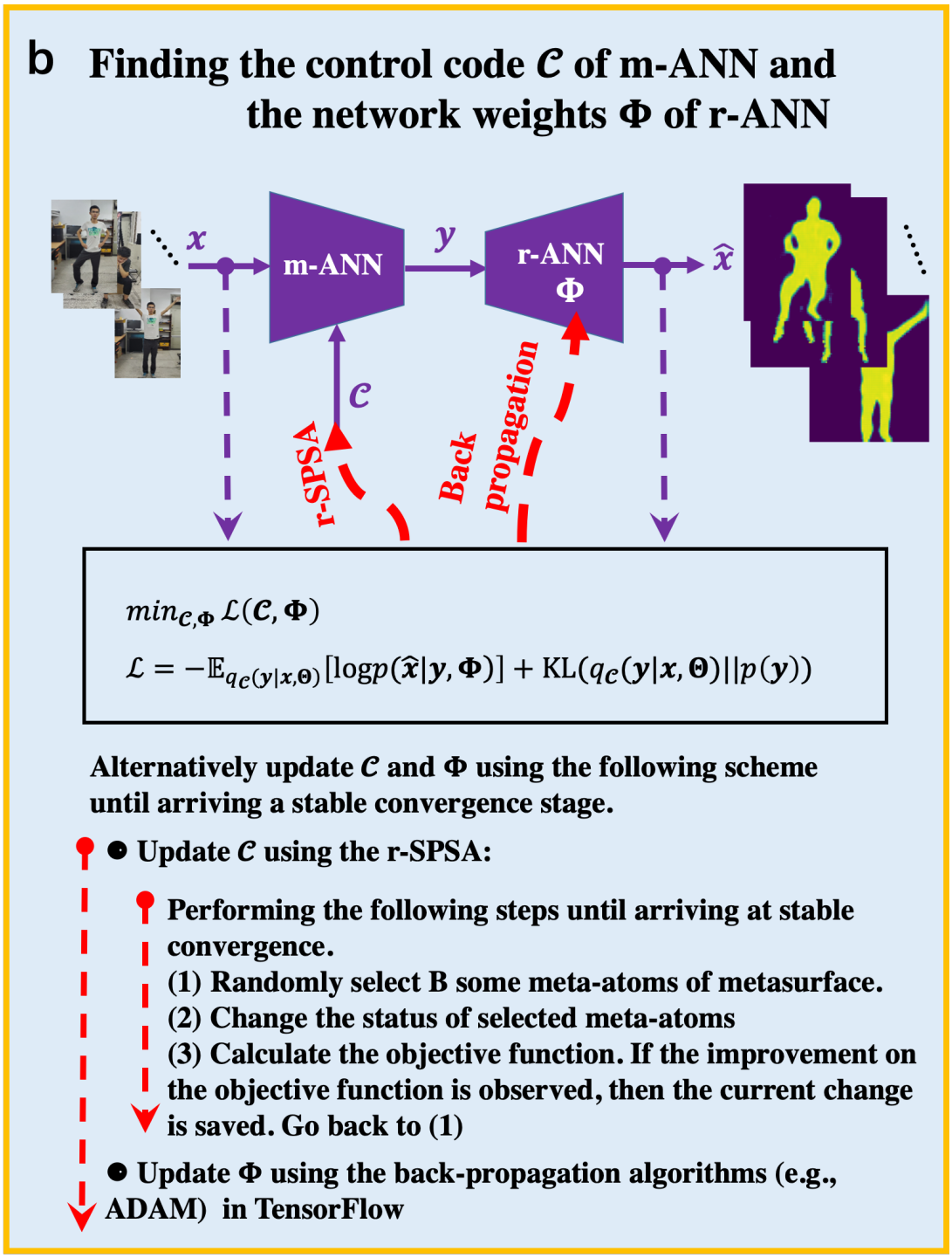


**Figure S2**. (a) the flow chart of learning the network weights of the m-ANN. (b) the flow chart of determining the optimal settings of the coding pattern of the metasurface and the network weights of the r-ANN.

In numerical implementation, the expectation term $-\mathbb{E}_{q_{\mathcal{C}}(y|x,\Theta)}[\log p(x|y,\Phi)]$ is

replaced by finite-sample statistical mean approximation over the training dataset. As for $\mathrm{KL}(q_{\boldsymbol{C}}(\boldsymbol{y}|\boldsymbol{x},\boldsymbol{\Theta})||p(\boldsymbol{y}))$, it can be analytically treated under the Gaussian assumption, as detailed in ref. 1 in main text. In addition, in our implementation, Eq. (S1) is slightly modified as following, i.e.,

$$\mathcal{L}(\boldsymbol{C},\boldsymbol{\Phi}) = -\mathbb{E}_{q_{\boldsymbol{C}}(\boldsymbol{y}|\boldsymbol{x},\boldsymbol{\Theta})}[\log p(\boldsymbol{x}|\boldsymbol{y},\boldsymbol{\Phi})] + \gamma \mathrm{KL}(q_{\boldsymbol{C}}(\boldsymbol{y}|\boldsymbol{x},\boldsymbol{\Theta})||p(\boldsymbol{y})) \quad \text{(S2)}$$

Here, $\gamma$ is introduced to tradeoff the contributions from the data misfit and the prior-based regularization.

It is noted that in minimizing Eq. (S1), it involves two sets of different optimization variables, i.e., the continuously adjustable weights $\boldsymbol{\Phi}$ in the r-ANN and $\boldsymbol{\Theta}$ in the m-ANN, and the binary controllable variables $\boldsymbol{\Theta}$ in the m-ANN. Apparently, the optimization with respect to $\boldsymbol{\Phi}$ and $\boldsymbol{\Theta}$ can be efficiently realized with the well-known back-propagation (BP) algorithm, which can be accomplished with well-developed optimizers in TensorFlow. However, it is really challenging to minimize Eq.(S1) with respect to the binary control coding sequences $\boldsymbol{C}$ since it involves a NP-hard combinatorial optimization problem. To surpass this difficulty, the randomized simultaneous perturbation stochastic approximation (r-SPSA), originally developed for the problem of optimal well place and control in area of petroleum engineering, is slightly modified for our problem. This heuristic optimization approach relies on two randomized descent strategies. First, as done by stochastic gradient descent approach, at each iteration, a fraction of training samples is randomly selected to determine a descent direction. Consequently, the concept of batch size is also applicable. Second, at each iteration, as done by so-called randomized coordinate descent method, only a fraction of optimization components chosen to be updated. Here, partial coding meta-atoms of metasurface are randomly selected, and their binary status are changed to their opposites correspondingly. If the change leads to the improvement on the objective function defined over randomly selected training samples, we save such change and go into next iteration. Otherwise, we need to randomly re-select some of coding meta-atoms of metasurface and perform above operations. Repeat such procedure until some stop criterion

is arrived. More details about the implementation of the proposed r-SPSA optimization algorithm can be seen in **Figure S2**.

## Supplementary Note 3. Experimental settings

In order to evaluate the contribution of the joint training of the measurement setup and data processing pipeline, we have designed a two-stage experiment. First, we train the reconstruction network alone while fix the measurement setting (i.e., the programmable metasurface with pre-specified control coding patterns). Second, we use a pre-convergence checkpoint of the reconstruction network as a starting point for the joint training. At this stage, both the reconstruction network and the measurement setting are jointly trained. In order to factor out the undesired influence of the optimization algorithm on the sensing results, we train the reconstruction network in both stages with the same optimizer (ADAM, batch-size=10, initial learning rate=0.005), and train the measurement setting (i.e., the control coding pattern of metasurface) using the r-SPSA algorithm (batch-size =200, and the number of elements each iteration=20).

For all the experiments throughout the paper, the *learned measurement* refers to the setting where the control coding pattern of programmable metasurface is trained alone and the reconstruction network is fixed; the *learned reconstruction* refers to the setting where the reconstruction network is trained alone, and the control coding pattern of programmable metasurface is fixed; the *learned measurement-reconstruction* refers to the setting where the control coding pattern of metasurface is jointly trained with the reconstruction network.

## Supplementary Note 4. Discussions about the m-ANN

Here, we would like to provide physical insights into the m-ANN by investigating its connection with the classical EM scattering mechanism. To that end, the investigation domain including the subject is uniformly divided into M subgrids, and each subgrid is

occupied by an ideal dipole. In light of coupled dipole method (CDM), when the probed subject is illuminated by an EM wavefield, the resultant scattering electrical wavefield at $\boldsymbol{r}$ outside the investigation domain is governed by the following equations:

$$E^{(sca)}(\boldsymbol{r}) = \sum_{m=1}^{M} \mathrm{G}(\boldsymbol{r}, \boldsymbol{r}_m)\alpha(\boldsymbol{r}_m)E(\boldsymbol{r}_m) \tag{S4}$$

and

$$E(\boldsymbol{r}_n) = E^{(inc)}(\boldsymbol{r}_n) + \sum_{m=1, m\neq n}^{M} \mathrm{G}(\boldsymbol{r}_n, \boldsymbol{r}_m)\alpha(\boldsymbol{r}_m)E(\boldsymbol{r}_m) \tag{S5}$$

$$n = 1,2,\dots,M$$

Herein, $\alpha(\boldsymbol{r}_m)$ represents the polarizability of the equivalent dipole at the location of $\boldsymbol{r}_m$, $E(\boldsymbol{r}_m)$ means the internal electrical field induced at $\boldsymbol{r}_m$, and $\mathrm{G}$ is the Green's function for surrounding background environment. $E^{(inc)}(\boldsymbol{r}_n)$ denotes the illumination radiated from the metasurface controlled with a control coding pattern. Note that we have explicitly made the scalar simplification in Eqs. (S4) and (S5) for the sake of simplicity, however, the methodology presented here can be extended to full-vectorial cases in a straightforward manner.

Now, our primary goal is to calculate $E^{(sca)}(\boldsymbol{r})$ given $\{E^{(inc)}(\boldsymbol{r}_n)\}$ and $\{\alpha(\boldsymbol{r}_m)\}$, where a critical issue is to estimate the intermediate variables $\{E(\boldsymbol{r}_n)\}$ by solving Eq.(S5). Once $\{E(\boldsymbol{r}_n)\}$ are known, the scattering wavefield $E^{(sca)}(\boldsymbol{r})$ can be obtained by using Eq. (S4). However, it is an open challenging issue to efficiently solve Eq. (S5) when the Green's function $\mathrm{G}$ cannot be treated in a tractable way. As a matter of fact, even if the $\mathrm{G}$ can be efficiently treated, it remains not an easy task to solve the large-scale problem of Eq. (S5) from the computational viewpoint, for instance, this inverse problem usually suffers from the notorious ill-posedness in the large-scale case. In the era of AI (Artificial Intelligence), ML techniques, especially deep learning, can be explored to address above difficulties. Particularly, with a standard supervised training procedure, a well-defined end-to-end mapping from $\{E^{(inc)}(\boldsymbol{r}_n)\}$ or $\{\alpha(\boldsymbol{r}_m)\}$ to $E^{(sca)}(\boldsymbol{r})$ can be learned from a number of labeled training data. In this section, we would like to investigate a connection between the solution to Eqs. (S4)-(S5) and the deep ANN, as outlined in **Figure S3**.

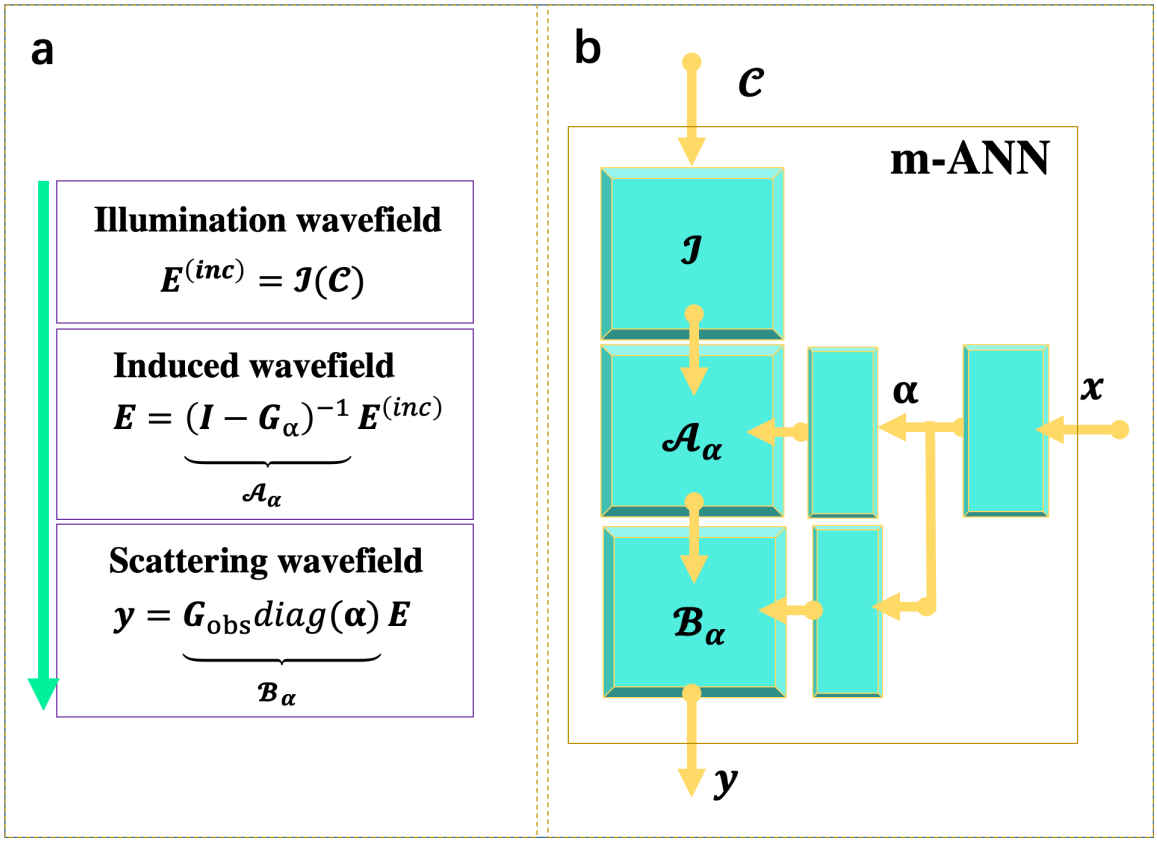


**Figure S3**. The connection between the proposed measurement procedure and the three-port m-ANN. (**a**), the acquired signal can be modelled with three cascaded networks. The first one is characterized by $\boldsymbol{E}^{(inc)} = \boldsymbol{\mathcal{I}}(\boldsymbol{\mathcal{C}})$, which relates nonlinearly the illumination wavefield $\boldsymbol{E}^{(inc)}$ to the coding pattern $\boldsymbol{\mathcal{C}}$ of the metasurface. Other two are α-dependent fully-connected networks which are mathematically characterized by $\boldsymbol{E} = (\boldsymbol{I} - \boldsymbol{G}_\alpha)^{-1}\boldsymbol{E}^{(inc)} = \mathcal{A}_\alpha \boldsymbol{E}^{(inc)}$ and $\boldsymbol{y} = \boldsymbol{G}_{\text{obs}} diag(\alpha)\boldsymbol{E} = \mathcal{B}_\alpha \boldsymbol{E}$, respectively. Here, $\boldsymbol{E} = \boldsymbol{G}_{\text{obs}} diag(\boldsymbol{\alpha})\boldsymbol{E}$ is a compact representation of **Eq.(S4)**. The dependence on α from these two fully-connected networks are further established with deep ANNs, as demonstrated in **Figure S3b**. (**b**) the deep ANN representation of (a). The polarizability distribution $\boldsymbol{\alpha}$ could be a linear or nonlinear function of the input scene $\boldsymbol{x}$. For instance, when $\boldsymbol{x}$ indicates the class label of the scene, $\boldsymbol{\alpha}$ will be nonlinearly related to $\boldsymbol{x}$ via a deep generative network. Such nonlinear mappings are modelled with deep CNNs in our work. Additionally, the nonlinear operator $\boldsymbol{\mathcal{I}}$ is also approximated by a deep CNN in our implementation.

First, we consider to solve Eq. (S5) by using the direct matrix inversion technique. To this end, we rewrite Eq.(S5) in a compact form as following, i.e.,

$$\boldsymbol{E} = \boldsymbol{E}^{(inc)} + \boldsymbol{G}_\alpha \boldsymbol{E} \tag{S6}$$

Herein, $\boldsymbol{E}$ and $\boldsymbol{E}^{(inc)}$ are M-length column vectors, in which the $n$th elements are $E(\boldsymbol{r}_n)$ and $E^{(inc)}(\boldsymbol{r}_n)$, respectively. $\boldsymbol{G}_\alpha$ denotes a α-dependent matrix with a size of $M \times M$,

whose diagonal entries are zero, and the (*n, m*)-entry is $\mathrm{G}(\boldsymbol{r}_n, \boldsymbol{r}_m)\alpha(\boldsymbol{r}_m)$. Apparently, Eq. (S6) can be solved with a matrix inversion, i.e.,

$$\boldsymbol{E} = (\boldsymbol{I} - \boldsymbol{G}_\alpha)^{-1}\boldsymbol{E}^{(inc)} \tag{S7}$$

Note that the wavefield $\boldsymbol{E}$ is linearly related to illumination $\boldsymbol{E}^{(inc)}$ through $(\boldsymbol{I} - \boldsymbol{G}_\alpha)^{-1}$. As argued above, it is more feasible to learn an agent for $(\boldsymbol{I} - \boldsymbol{G}_\alpha)^{-1}$ with ML techniques than calculate it directly. Furthermore, the matrix $(\boldsymbol{I} - \boldsymbol{G}_\alpha)^{-1}$ varies with $\alpha$ in a nonlinear way. Here, we would like to emphasize that the illumination wavefield $\boldsymbol{E}^{(inc)}$ depends on the control coding pattern of metasurface $\boldsymbol{C}$, and that the polarizability $\alpha$ characterizes the subject. In order to establish the nonlinear relation mapping from $\alpha$ to $(\boldsymbol{I} - \boldsymbol{G}_\alpha)^{-1}$, a standard ANN can be used as well. In addition, the illumination wavefield $\boldsymbol{E}^{(inc)}$depends nonlinearly on the control coding pattern of metasurface $\boldsymbol{C}$, and such nonlinear operator can be modeled with a standard end-to-end ANN as well. Inspired by these observations, we introduce a three-port ANN for charactering the whole measurement procedure of the proposed sensing system, as outlined in **Figure S3**. The resultant ANN has three ports: one is used to receive the scene properties, i.e., $\alpha(\boldsymbol{r}_m)\}$, one is for the control coding pattern of metasurface $\boldsymbol{C}$, and the other is for outputting the microwave raw data $\boldsymbol{y}$. Such three-port measurement ANN can be learned with a standard supervised training procedure.

## Supplementary Note 5. Comparing with PCA-based measurements

The proposed full-ANN-driven intelligent sensing strategy works in a nonlinear ML way, as opposed to PCA (linear) technique. Here, we would like to highlight two major benefits of our sensing technique over PCA method. First, since the PCA approach requires an analytical measurement model, one may obtain the superior performance of our sensing strategy in any scenario where the PCA approach could be applicable, from the viewpoint of computational efforts. Second, the ability to synthesize the PCA measurement modes is highly dependent on the number of metasurface meta-atoms, implying that the PCA approach is suitable only for scenarios where the number of metasurface meta-atoms is

really large.

In our experiments, the coding patterns of the metasurface are initialized using the PCA method, and then jointly optimized along with the r-ANN. The significant improvement on the objective function can be clearly observed, especially when the number of control coding patterns M is very limited. Correspondingly, the imaging results can be clearly improved with our method, highlighting our method's unique ability to perform sensing tasks with respect to the PCA method. This does make sense since the presented intelligent sensing approach has more controllable degrees of freedom, and accounts for more prior knowledge about the scene, the data measurement and processing into the entire sensing chain, as opposed to the PCA approach which only considers the prior information on the scene.

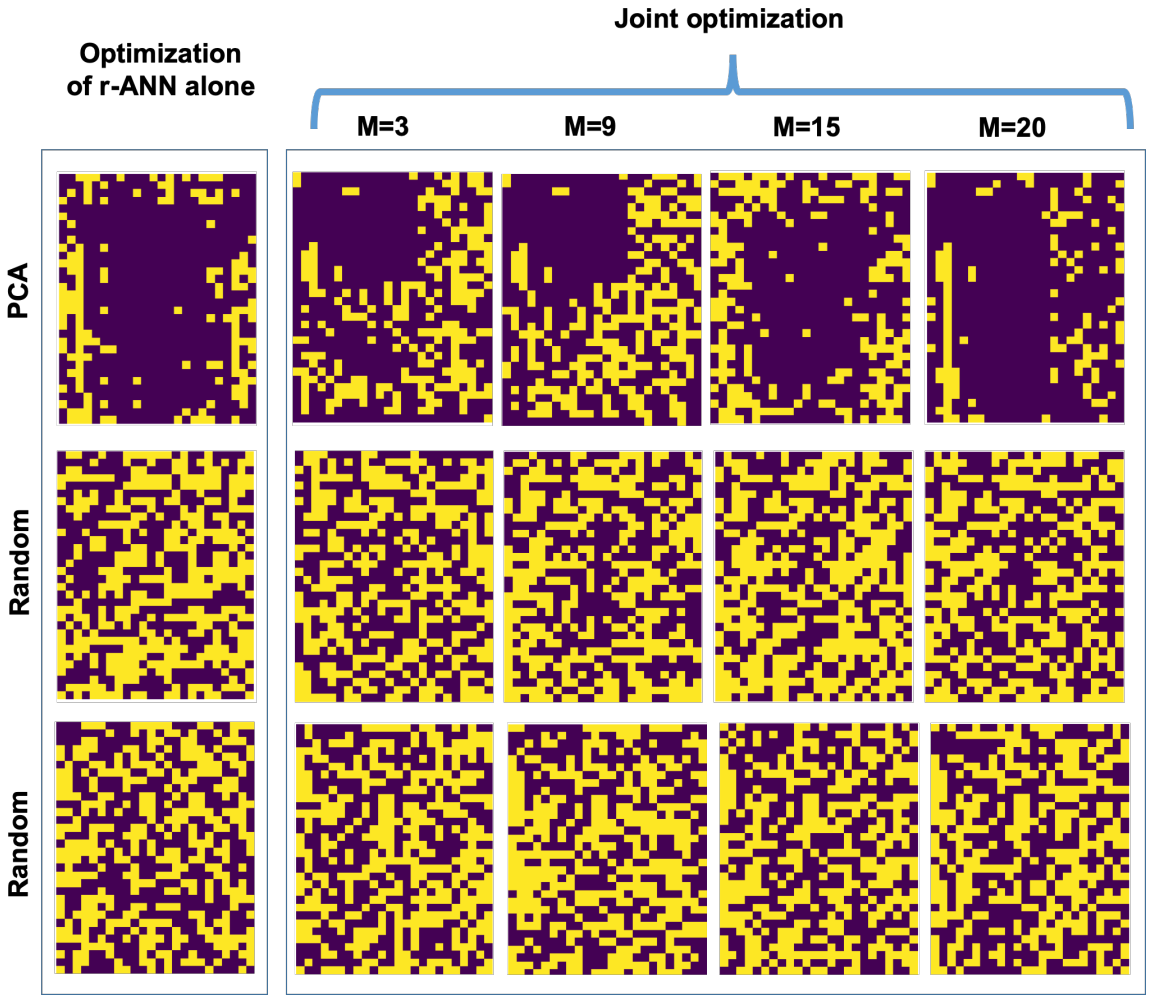


**Figure S4**. Selected optimized coding patterns of the metasurface, corresponding to that involved in Figure 2 in main text. From these figures, it can be observed that the coding patterns of the metasurface are remarkably changed when the measurements are highly limited.

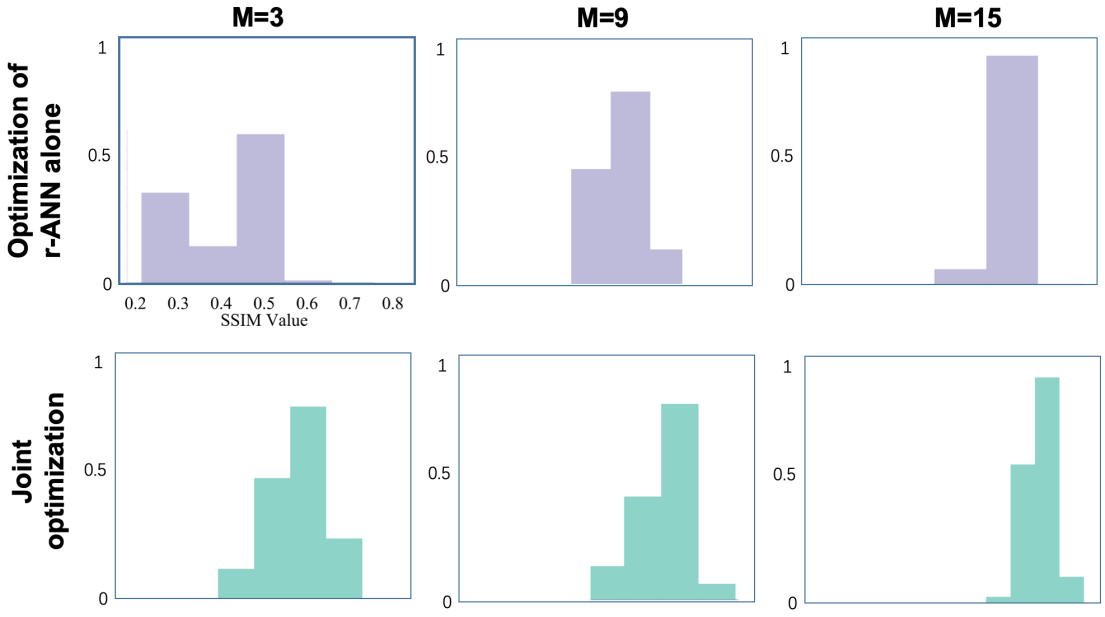


**Figure S5**. The dependences of the SSIMs of the images obtained by different sensing methods on the number of coding patterns M of the programmable metasurface. These results correspond to Figures 2 and 3 in main text.